Climatic Change (2020) 162:1323–1343
https://doi.org/10.1007/s10584-020-02786-3

Can stratospheric geoengineering alleviate global warming-induced changes in deciduous fruit cultivation? The case of Himachal Pradesh (India)

Jyoti Singh, et al. *[full author details at the end of the article]*

Received: 13 August 2019 / Accepted: 2 July 2020 / Published online: 7 July 2020

Abstract
Using Hadley Global Environment Model 2 - Earth System and Max Planck Institute Earth System Model simulations, we assess the impact of global warming and stratospheric geoengineering on deciduous fruit production in Himachal Pradesh (the second-largest apple-producing state in India). The impacts have been assessed for the Representative Concentration Pathways 4.5 (RCP4.5) global warming scenario, and a corresponding geoengineered scenario (G3) from the Geoengineering Model Intercomparison Project, in which stratospheric aerosols are increased for 50 years from 2020 through 2069 to balance the global warming radiative forcing, and then aerosol precursor emissions are terminated. We used the period 2055–2069 (with the largest geoengineering forcing) and the period 2075–2089 (beginning 5 years into the termination phase) and evaluated winter chill and growing season heat accumulation. We found that although stratospheric geoengineering would be able to suppress the increase in temperature under an RCP4.5 scenario to some extent during both switch-on and switch-off periods, if the geoengineering was terminated, the rate of temperature increase would be higher than RCP4.5. The agroclimatically suitable area is projected to shift northeastwards (to higher elevations) under RCP4.5 as well as G3 during both periods. However, during the switched on period, geoengineering would restrict the shift, and areas of Shimla and Mandi districts (most suitable under the current climate) would not be lost due to global warming. Even during the switched off period, before the climate returned to RCP4.5 levels, the above areas would, although to a lesser extent, have reduced harmful climate effects from global warming. However, the area of suitable land (the intersection of soil and agroclimatic suitability) would decrease in both periods for RCP4.5 as well as G3, because as more high-elevation regions become agroclimatically suitable, they do not have suitable soils to support cultivation. Geoengineering could benefit deciduous fruit production by reducing the intensity of global warming; however, if geoengineering was terminated abruptly, the rate of change in temperature would be quite high. This could lead to a rapid change in land suitability and might result in total crop failure in a shorter period compared to RCP4.5.

Keywords Global warming · Geoengineering · Agroclimatic suitability · Deciduous fruit production · Soil suitability

Electronic supplementary material The online version of this article (https://doi.org/10.1007/s10584-020-02786-3) contains supplementary material, which is available to authorized users.

1 Introduction

Anthropogenic climate change is a fact, and its consequences are affecting almost all components of our ecosystem. Various studies have shown that climate change may affect the growing season for crops, moisture regimes, and crop micro-climates and canopy characteristics, and hence may play a significant role in altering cropping patterns and crop suitability across the globe (Olesen and Bindi 2002). Since agriculture over a given region is dependent on the local climate, the suitability of different regions for growing various crops may either increase or decrease due to the changing climate (IPCC 2014). To adapt to the likely impacts of climate change, it is necessary to study the land and climate suitability for sustainable agriculture (Bhagat et al. 2009; Tuan et al. 2011; Kihoro et al. 2013).

The Himalayan region, known as the Third Pole, has a fragile ecosystem and tremendous diversity, thus making it vulnerable to climate change (Chaudhary and Bawa 2011; Shrestha et al. 2012). It has been facing climate change challenges due to warmer winters, irregular precipitation, increased aridity and increased frost, and storm events (Dash and Hunt 2007), leading to severe impact on horticulture and agriculture practices (Renton 2009). Deciduous fruits such as apple, cherry, apricot, peach, and pear are important harvests of the Himalayan region (Ghosh 1999). Himachal Pradesh, one of the largest producers of apples in India, located in the Himalayas, extends from 30° 22′ to 33° 12′ N and from 75° 45′ to 79° 04′ E, stretching over 55,673 km^2 (Fig. 1). Himachal Pradesh can be segregated into five distinct physiographic regions, namely, the Greater Himalayas or Alpine zone, the Lesser Himalayas, the outer Himalayas (or the Shivaliks), piedmont plains, and flood plains. In this region, very diverse climatic conditions are witnessed from hot and sub-humid tropical to temperate, cold alpine and glacial, due to variation in elevation (~350–7000 m), and aspect. Apple-growing areas in Himachal Pradesh do not fall within the temperate zone of the world, but its temperate climate due to high altitude provides sufficient winter chill as required by apple and other deciduous fruits.

As reported in many experiments for deciduous fruit trees, a period of sufficiently low temperatures (chill accumulation) followed by a period of warm temperatures (heat accumulation) is required for proper bud burst along with adequate flowering and fruit ripening (Richardson et al. 1974; Erez 2000; Ikinci et al. 2014). Deciduous fruit trees stay dormant by reducing activity in winters and then resume growth after completing the rest period by accumulating a sufficient chill (Cesaraccio et al. 2004; Luedeling and Brown 2011). By accumulating sufficient winter chill, the plants prepare for the exposure to subsequent springtime warming, crucial for adequate fruit development (Schwartz and Hanes 2010). However, a rigorous understanding of the relation between physiological mechanisms, winter chill, and heat requirements is not established (Cesaraccio et al. 2004; Atkinson et al. 2013). Climate change may lead to inadequate chill and heat accumulation, thus affecting the site suitability of deciduous fruit species, and hence affecting productivity (Cesaraccio et al. 2004; Luedeling and Brown 2011).

Several studies have been carried out in the past to quantify chill and heat accumulation of deciduous fruits. In most of these studies, primarily, three models have been used to predict the chill requirement: (i) chill hour model that counts hours below specific chilling temperature, (ii) chill unit model that counts weighted units below specific temperatures, and (iii) dynamic model that takes a different approach to quantify winter chill (Richardson et al. 1974; Fishman et al. 1987; Linvill 1990; Linkosalo 2000). There have been studies that applied chill models to investigate the impact of climate change on phenology, bud burst time, and productivity

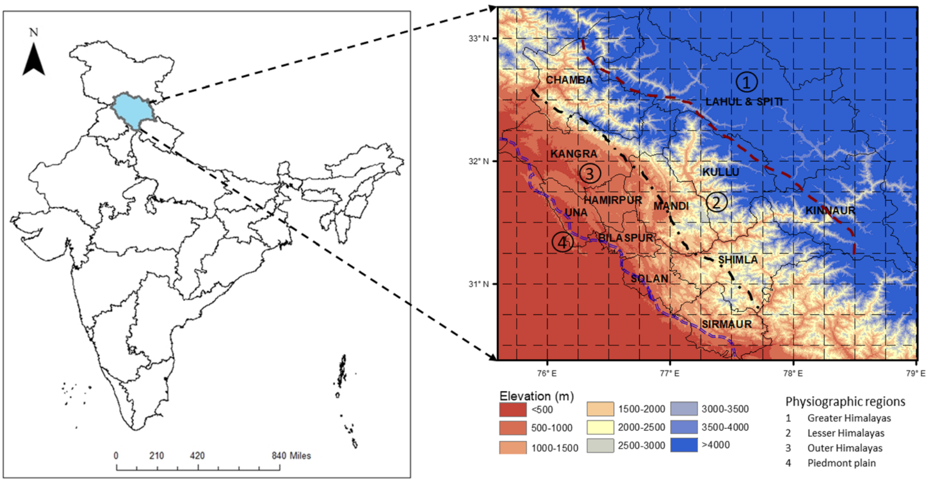

Fig. 1 Location of the study area (Himachal Pradesh, India). The dotted lines (violet, black, and red) divides the four physiographic regions (Greater Himalayas, Lesser Himalayas, Outer Himalayas, and Piedmont plains). The overlaid grid boxes represent the resolution (25 km) at which the study is carried out

(Cesaraccio et al. 2001; Luedeling and Brown 2011; Kishore et al. 2015; Rana et al. 2015; Singh and Patel 2017). In some of the studies along with the chill model, a heat model (e.g., growing degree hours (GDH)) is also combined to calculate both chilling and thermal requirement, as both are crucial to break dormancy and resume proper growth conditions (Guo et al. 2015; Santos et al. 2017). In this study, we have used the dynamic model along with the GDH model to analyze adequate growing condition by measuring chill accumulation in winters and heat accumulation in spring, respectively.

There have been various studies on the impact of global warming on winter chill and the productivity of deciduous fruit trees. Luedeling et al. (2009b) quantified winter chill in California for observed historical and projected future climate using chilling hours and a dynamic model. Their study projected winter chill to decrease by 50–70% by mid-century and as high as 90–100% by the end of the twenty-first century. The study recommended strong adaptation strategy requirements for the California valley. Santos et al. (2017) combined GDH and dynamic models to assess thermal growing conditions for temperate fruits in Portugal for historical observations, RCP4.5, and RCP8.5. A decrease in the winter chill and an increase in GDH were projected, and the need for adaptation strategies was suggested to cope with climate change. Rana et al. (2015) applied the Utah chill unit model and the Ashcraft model to examine the shift in the apple belt in Himachal Pradesh in recent years using climate data and fruit growers perception. They found that apple cultivation is becoming suitable at higher altitudes due to increased winter chill, whereas the opposite is true for lower elevation areas.

Among measures to combat global warming, geoengineering is being studied as one possible scheme. Kravitz et al. (2011) proposed four experiments (G1, G2, G3, and G4) as part of the Geoengineering Model Intercomparison Project (GeoMIP) to assess the impact of stratospheric geoengineering with selected general circulation models (GCMs) as part of the Coupled Model Intercomparison Project Phase 5 (CMIP5) experiments under various global warming scenarios. There are many potential risks of geoengineering that would play an equally important role in deciding the pros and cons if such an initiative was to be carried out anytime in the future (Robock 2016). In the context of agricultural impacts, Pongratz et al.

(2012) showed that overall yield of maize, rice, and wheat would increase if CO_2 was doubled, but temperatures were kept from increasing with solar radiation management (SRM) because of reduction in heat stress and positive CO_2 fertilization. A similar study by Xia et al. (2014) for maize and rice crops in China, using outputs from 10 GCMs that participated in GeoMIP, supports the outcomes of Pongratz et al. (2012). They reported that maize yield could increase, but rice yield would remain the same because of SRM. Yang et al. (2016) used outputs for historical, RCP4.5, and the G3 scenario to analyze the impact of geoengineering on groundnut yield over India. Groundnut yield was projected to decrease by 20% in geoengineering period of 50 years from 2020 to 2070, and upon switching off geoengineering yield reverted to non-geoengineered values within a few years.

The aim of this study is to assess the change in the suitability of various deciduous fruit trees from the present climate to RCP4.5 and G3 (geoengineered; described in the next section) scenarios. The methodology is as follows: (1) bias correction of GCM simulations; (2) statistical downscaling of the bias-corrected GCM data to finer resolution; (3) converting daily temperature data into hourly data; (4) calculating chilling and heat accumulation using chill and heat models for historical, RCP4.5, and G3 scenarios; (5) assessing the change in thermal conditions for the above scenarios; and (6) evaluating the shift in site suitability of the important deciduous fruits by taking into account the corresponding soil suitability along with agroclimatic suitability for the above scenarios.

2 Data and methods

2.1 Data

In the G3 scenario, the radiative forcing in RCP4.5 is used in combination with stratospheric geoengineering (injecting aerosols in the lower stratosphere). G3 and RCP4.5 differ in terms of radiative forcing and surface temperature. A total of six models participated in G3 (BNU-ESM, GISS-E2-R, HadGEM2-ES, IPSL-CM5A-LR, MPI-ESM-LR, and NorESM1-M). In a study by Ferraro and Griffiths (2016), they used only HadGEM2-ES and MPI-ESM-LR for the G3 scenario and did not use the other models for the following reasons. In IPSL-CM5A-LR, radiative transfer calculations did not include the infrared effects of stratospheric sulphate aerosol. In NorESM1-M, a bug was found in calculating of the infrared effects of stratospheric sulphate aerosol. BNU-ESM and GISS-E2-R were excluded because the RCP4.5 and G3 experiments were performed for each of these models in different computational environments, thus producing different climates, so it is not possible to compare them. Our choice of HadGEM2-ES and MPI-ESM-LR is also influenced by the fact that these models are some of the best performing CMIP5 models over the region of interest (Mishra et al. 2018).

Therefore, to study the impacts of global warming under RCP4.5 and G3 on chill and heat accumulation of deciduous fruits, the model output from the Hadley Centre Global Environment Model version 2 – Earth System (HadGEM2-ES; Collins et al. 2011) and the Max-Planck-Institute Earth System Model – Low Resolution (MPI-ESM-LR; Giorgetta et al. 2013) have been used. For the historical and global warming analysis, we have used the RCP4.5 simulations from CMIP5 (Taylor et al. 2012), and for the geoengineering analysis, we have used model data from the G3 dataset of GeoMIP (Kravitz et al. 2011). The historical model data (Hist) are available for the period 1909–2005, and the RCP4.5 data are analyzed for the period 2006–2099. The geoengineering data (G3) are available for 2020–2089. In the historical runs, CO_2 levels used are those observed during the corresponding historical period. In the RCP4.5 runs, CO_2 levels increase from 380 ppm in 2006 to 538 ppm in 2099. In the G3 experiment, SO_2 is added gradually in the stratosphere (at one point at the equator), branching of the RCP4.5 runs starting in 2020, to create sulphate aerosols to neutralize the increase of the corresponding global mean radiative forcing due to increased CO_2 levels in RCP4.5. Although G3 stops the increase of global mean radiative forcing from RCP4.5 when geoengineering is switched on, there will still be small global mean surface temperature changes due to the small unrealized radiative imbalance (< 1 W m^{-2}) at the time the SO_2 emissions begin in 2020. Regional changes in surface temperature and other climate variables induced by this warming will also occur. G3 simulations start in 2020 and end in 2089. However, the sulphate aerosol injection is ceased after 2069 (Kravitz et al. 2011).

The daily maximum, minimum, and mean temperatures used in this study are from the Princeton Global Forcing's observational-reanalysis hybrid data freely available from the Terrestrial Hydrology Research Group of Princeton University (Sheffield et al. 2006). Daily maximum, minimum, and mean 2 m air temperature at 0.25° grid resolution for period 1 January 1948 to 31 December 2008 have been used in this study and were downloaded from the website http://hydrology.princeton.edu/data/pgf/0.25deg/daily/. The India Meteorological Department provides observed daily temperature (maximum, mean, and minimum) data in the gridded form at 1° grid resolution (Srivastava et al. 2009). However, Himachal Pradesh is complex hilly terrain and 1° grid resolution is too coarse to represent the spatial structure of temperature. The Asian Precipitation Highly-Resolved Observational Data Integration Towards Evaluation (Yasutomi et al. 2011) dataset provides observed daily mean temperature data at 0.25° grid resolution; however, since we also need daily maximum, and minimum temperature to produce hourly temperature, the Princeton temperature dataset was chosen.

We have also used the soil map at 1:250000 scale published by the National Bureau for Soil Survey and Land Use Planning (NBSS&LUP; Sehgal 1990). The soil attributes in the soil map database are unit id, soil depth, drainage, particle size, slope, erosion, surface stoniness, flooding, calcareousness, salinity, and sodicity.

For topography analysis of Himachal Pradesh, the Shuttle Radar Topographic Mission (SRTM) topographic data were used. The Digital Elevation Model (DEM) from this mission covers on a near-global scale from 56° S to 60° N to generate the most complete high-resolution digital topographic database of Earth. SRTM data are available at the finest resolution of 1 arcsec (nearly 30 m), but in this study, 1-km resolution SRTM DEM data (Becker et al. 2009) were used and were downloaded from https://dds.cr.usgs.gov/srtm/version2_1/SRTM30/.

2.2 Bias correction

Although HadGEM2-ES and MPI-ESM-LR have been reported to perform better than most of the CMIP5 models over the region of interest (Mishra et al. 2018), they still have some biases which need to be corrected before carrying out our analysis. Hence, we first bias corrected the model data before using them for analysis. We have applied a widely used bias correction method known as Quantile Mapping (QM); e.g., (Gudmundsson et al. 2012) on Hist, RCP4.5, and G3 data. Daily maximum, minimum, and mean temperatures from Princeton Global Forcing were resampled at the grid resolution of HadGEM2-ES (1.875° × 1.25°) and MPI-ESM-LR (1.875° × 1.667°). The QM method fine-tunes the daily distribution of model data with the observed distribution for each of the variables from both the models. The model and the resampled Princeton data contain a total of 12 (3 × 4) grid boxes for HadGEM2-ES and 9 (3 × 3) grid boxes for MPI-ESM-LR for capturing entire Himachal Pradesh. The data are divided into 0.25 percentile cumulative distribution function (CDF) bins. For every bin, a transfer function is calculated from the ratio of corresponding percentile values of resampled Princeton and model data (separately for HadGEM2-ES and MPI-ESM-LR for the period 1971–2005). The computed transfer function is then applied to all the data points of the model data in the corresponding bins to obtain the bias-corrected model data.

2.3 Statistical downscaling

Given that the model data are at a much coarser resolution as compared with what one would need to assess the impacts of warming and geoengineering on deciduous fruit cultivation over Himachal Pradesh (having complex terrain and micro-climates), we performed a statistical downscaling on the bias-corrected model data. We have used the QM approach for statistically downscaling the model data using the relationship between coarser (bias corrected GCM data) and finer (Princeton data) space scales. Both of the models have different grid resolution and contain a different number of grid boxes (see Section 2.2 for details) for Himachal Pradesh. The Princeton data (0.25°) and model data (1.875° × 1.25° and 1.875° × 1.667° for HadGEM2-ES and MPI-ESM-LR, respectively) were divided into 0.25 percentile CDF bins. Princeton's fine resolution data grid was mapped to the containing/ nearest model's coarse resolution grids. At a given percentile bin in the CDF, the transfer function (a measure of the relationship between the coarse and the fine-scale) is computed from the ratio of the corresponding percentile values of the Princeton and the model data (separately for HadGEM2-ES and MPI-ESM-LR). Say, for example, for a given grid point in the 0.25° domain, the transfer function for data points between 10 and 10.25 percentiles (denoted as the 10.125 bin) can be computed by dividing the 10.125th percentile value from a Princeton data grid by the corresponding 10.125th percentile value from the mapped model grid. This transfer function is then applied to all data points of the coarse model output that fall in the corresponding 10.125 bin, thus resulting in a statistically downscaled dataset at a resolution of Princeton data. The downscaled data (for HadGEM2-ES and MPI-ESM-LR) and Princeton data were extracted for the Himachal region, resulting in 168 (12 × 14) grid boxes.

In Fig. 2, we have compared the statistically downscaled versions of daily maximum (a, b, c), mean (d, e, f), and minimum (g, h, i) temperatures from model data (HadGEM2-ES and MPI-ESM-LR) with observations. As can be seen from the figure, the finer scale features that are entirely missing in the coarse model data (Supplementary Fig. I) now mimic the observed spatial temperature pattern (Princeton) closely. For example, as seen in Fig. 1a, the Kullu district has a daily maximum temperature ranging from 4 to 20 °C for Princeton; however, this range shrinks to 12 to 16 °C in HadGEM2-ES data and 8–16 °C in MPI-ESM-LR (Supplementary Fig. I (b, c)) due to coarse resolution. After downscaling (Fig. 2b), the model daily temperature range closely mimics the values seen in the Princeton data.

2.4 Hourly temperature conversion

Given that the chill model (dynamic model) and forcing model (GDH) require hourly weather data as input, a method is used to estimate hourly temperature data from given daily temperature data. The widely used temperature model (TM) (Cesaraccio et al. 2001) framework was chosen to estimate hourly temperature.

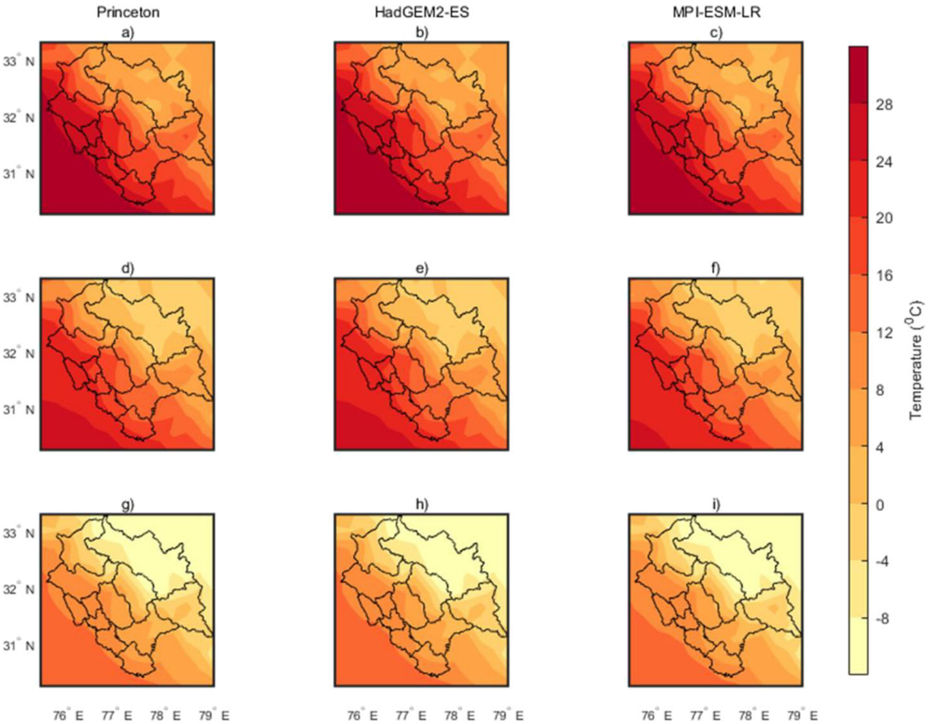

Fig. 2 Daily maximum temperature (a, b, c), daily mean temperature (d, e, f), and daily minimum temperature (g, h, i) for Princeton global forcing data, downscaled HadGEM2-ES, and downscaled MPI-ESM-LR respectively

The TM model divides the day into three segments to estimate hourly temperature. From the sunrise hour (*Hn*) to the time of maximum temperature (*Hx*), from *Hx* to the sunset hour (*Ho*), which uses a sine wave function, and from *Ho* to the sunrise hour of next day (*Hp*), a square root function is used to calculate the hourly temperature. *Hn* and *Ho* are site specific and depends upon the latitude and day of the year, $Hp = Hn + 24$ and $Hx = Ho - 4$.

Inputs of the model are the temperature at *Hn* (*Tn*), *Hx* (*Tx*), *Ho* (*To*), and *Hp* (*Tp*). *Tn* and *Tx* are minimum and maximum temperature, respectively, *To* is the temperature at sunset, and *Tp* is the temperature at the time of sunrise of the next day.

$$To = Tx - c\,(Tx - Tp) \tag{2.1}$$

where $c = 0.39$.

The TM model estimates hourly temperature using the following equations:

$$T(t) = \begin{cases} Tn + \alpha \sin\left[\left(\frac{t-Hn}{Hx-Hn}\right)\right]\frac{\pi}{2} & Hn < t \le Hx \\ To + R\sin\left[\frac{\pi}{2} + \left(\frac{t-Hx}{4}\right)\frac{\pi}{2}\right] & Hx < t < Ho \\ To + b\sqrt{t-Ho} & Ho < t \le Hp \end{cases} \tag{2.2}$$

where

$$\alpha = Tx - Tn \tag{2.3}$$

$$R = Tx - To \tag{2.4}$$

$$b = \frac{Tp - To}{\sqrt{Hp - Ho}} \tag{2.5}$$

Sunrise and sunset time are estimated using latitude, longitude, UTC coefficient, and date information.

2.5 Calculating chill and heat requirements

The chill requirement can be measured using chill portions, chilling hours, and chill units. Traditionally, chilling hours are estimated by counting the number of hours below a particular air temperature and chill unit is calculated by assigning a weight to chilling hours depending upon the air temperature range. The chill hour model (Chandler 1942) and chill unit (Utah) model (Richardson et al. 1974) are some examples of such models. The dynamic model, developed in Israel (Fishman et al. 1987; Erez et al. 1990), corrects the impact of high temperatures in the tropical region while calculating chill accumulation. The dynamic model performs better or at least equivalent to all the other models (Pérez et al. 2008; Luedeling et al. 2009a; Santos et al. 2017). Hence, the dynamic model is often considered as the best existing model for most regions of the world to compute chill requirement in the unit of chill portions (CP) because the classical chill hour and chill unit model are inadequate for subtropical climate regions. These models do not discriminate between temperate and subtropical climates appropriately because of their inability to consider impacts of high temperatures in winter on chill accumulation.

We choose the dynamic model to calculate chill accumulation in the form of CP along with the GDH model to estimate heat accumulation in the form of GDH. Usually, the chill accumulation season starts from late fall or early winter, and these chill models are used to predict the release of dormancy. In our study, the period of winter chill accumulation is taken from October to March and heat accumulation from April to September. The description of each model is given below:

The dynamic model, originally developed to consider high winter temperatures in Israel, takes a different approach to quantify winter chill. This quantification is based on the hypothesis that chill accumulation occurs in two stages to form chill portions. The first step has an intermediate product by some amount of cold temperature but can be nullified if warm temperatures occur. However, as soon as the chill accumulation crosses a certain threshold, it is converted into irreversible CP and is fixed.

To calculate GDH, two cosine functions are applied: (a) when *Ti* (hourly temperature) lies between *Tb* (base temperature (4 °C)) and *Tu* (optimal temperature (25 °C)) and (b) when *Ti* lies between *Tu* and *Tc* (critical temperature (36 °C)). GDH is zero if either *Ti* is less than *Tb* or *Ti* is higher than *Tc*.

$$
\mathrm{GDH} = \begin{cases} F\left(\frac{Tu-Tb}{2}\right)\left(1+\cos\left(\pi+\pi\frac{Ti-Tb}{Tu-Tb}\right)\right) & , \quad Tu \geq Ti \geq Tb \\ F(Tu-Tb)\left(1+\cos\left(\frac{\pi}{2}+\frac{\pi}{2}\frac{Ti-Tu}{Tc-Tu}\right)\right) & , Tc \geq Ti \geq Tu \\ 0 & , Ti > Tc \text{ or } Ti < Tb \end{cases} \tag{2.6}
$$

where $F = 1$ (as taken generally).

3 Results

3.1 Changes in surface temperature under RCP4.5 and G3

HadGEM2-ES and MPI-ESM-LR outputs from CMIP5 and GeoMIP were used to project changes in future daily maximum, mean, and minimum temperatures over Himachal Pradesh, using RCP4.5 and G3 scenarios. The differences of maximum, mean, and minimum temperatures under RCP4.5 and G3 from Hist are plotted in Figs. 3 and 4 for period 1 (2055–2069) and period 2 (2075–2089), respectively. The spatial range of temperature change is reported in Table 1. There is an increase in temperature up to 3.5 °C in period 1 and 4.5 °C in period 2 under RCP4.5. Although G3 is able to suppress the increase in temperature under the RCP4.5 scenario by around 1.0–1.2 °C for both the models in period 1 (geoengineering switched on), a significant fraction of the warming remains. Warming due to increasing greenhouse gas concentration impacts various regions of the world differently (Mann et al. 1998). Similarly, geoengineering stabilizes the ongoing radiative forcing to keep the global temperatures nearly constant; however, it may have distinct regional effects on temperature.

In period 2 (geoengineering switched off), the G3 temperatures are closer to RCP4.5 in both the models. Maximum, mean, and minimum temperatures in MPI-ESM-LR remain almost the same as in period 1 with a slight increase of around 0.1–0.2 °C. HadGEM2-ES temperatures vary significantly in period 2 as compared with period 1.

3.2 Changes in chill and heat requirement under RCP4.5 and G3

The orography of Himachal Pradesh is complex, ranging from ~350 to 7000 m. Flat terrain prevails in lower southern Himachal Pradesh, whereas steep slope terrain is characteristic of the upper northern Himachal region. Due to a wide range of climate, vegetation, landform, and geology, the state has a variety of soil. The flat terrain and lesser Himalayas have a large area of suitable soils, whereas the steep slope terrain of greater Himalayas has much less suitable soil. We combined SRTM DEM and NBSS&LUP soil maps to construct Fig. 5 which represents various elevation classes along with suitable soil for cultivation. Texture and depth are the properties considered to delineate the suitability of the soil for the farming of deciduous fruits. The NBSS&LUP vector map was converted to point features of 10-km resolution and overlaid over the DEM map. The state was then further divided into regions (I, II, and III). Regions I, II, and III mostly consist of areas with elevation less than 1500 m, ranging between 1500 and 4000 m, and higher than 4000 m, respectively. The chill accumulation occurs in winter (October–March), and heat accumulation takes place during spring (April–September). Therefore, chill accumulation will be referred to as winter chill and heat accumulation as spring heat from now on in this paper.

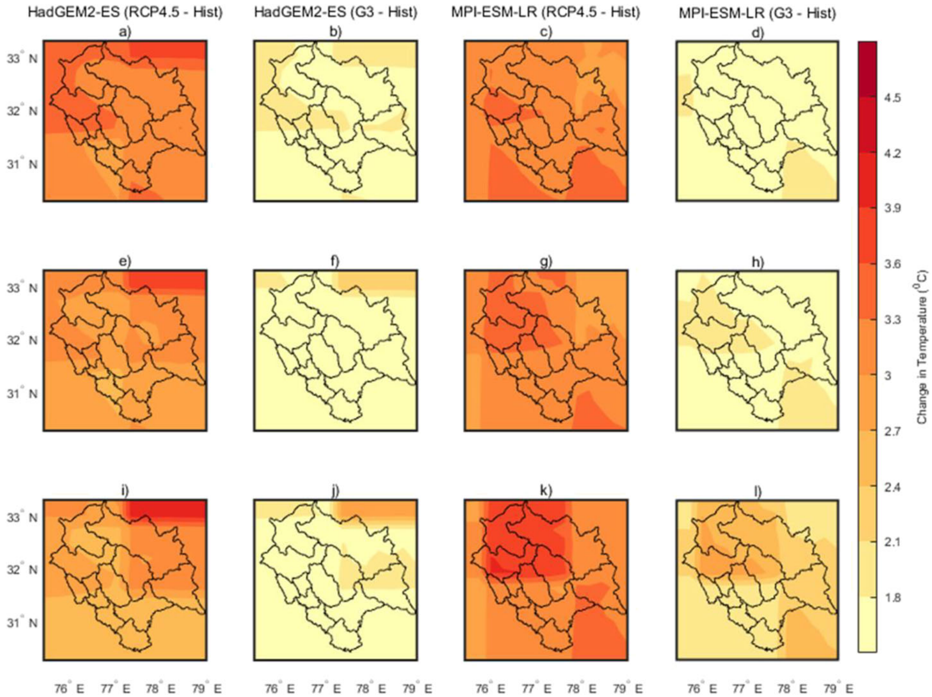

Fig. 3 Simulated changes in daily maximum temperature (a, b, c, d), daily mean temperature (e, f, g, h), and daily minimum temperature (i, j, k, l) under RCP4.5 and G3 for HadGEM2-ES and MPI-ESM-LR for period 1 (2055–2069; geoengineering switched on)

Deciduous fruit trees remain dormant during winter and exhibit no growth. The dormancy of the trees is complete if they experience adequate low temperatures for a specific period. These temperatures are converted into CP through the dynamic model to measure the amount of winter chill. Once the tree comes out of dormancy, it requires a sufficient amount of heat to resume proper growth. The spring heat is measured in the form of GDH. Winter chill and spring heat are plotted for HadGEM2-ES and MPI-ESM-LR and for the average of both in supplementary Fig. V. The distinct pattern of CP (Supplementary Fig. V a, b, c) can directly be correlated with the regions I, II, and III (Fig. 5). To explain this, we need to understand the connection between elevation, temperature, and CP. Himachal Pradesh does not fall in temperate zones of the world; the low temperatures required for the cultivation of deciduous fruits acquired in this region are because of high elevations. Region I consist of the lowest-lying areas (< 1500 m) and exhibits warmest temperatures, lower CP values (< 70 CP), and high GDH values. Region II (Chamba, Kullu, and Shimla districts) has elevations ranging between 1500 and 4000 m, the highest CP values (80–125) and adequate GDH. Region III situated above 4000 m acquires low CP and inadequately little GDH (< 8000). The winter chill is computed for the winter season (October–March) and spring heat for summers (April–September). The low values of CP in regions I and III are because of high temperature (above the threshold) and frigid temperatures (below the threshold), respectively. Region II has the highest CP values because it has adequate temperatures suitable to contribute to CP. With respect to GDH, regions I and II both acquire a sufficient amount of GDH (40,000–70,000) as the summer temperatures are well above 4 °C and below 36 °C, whereas region III has

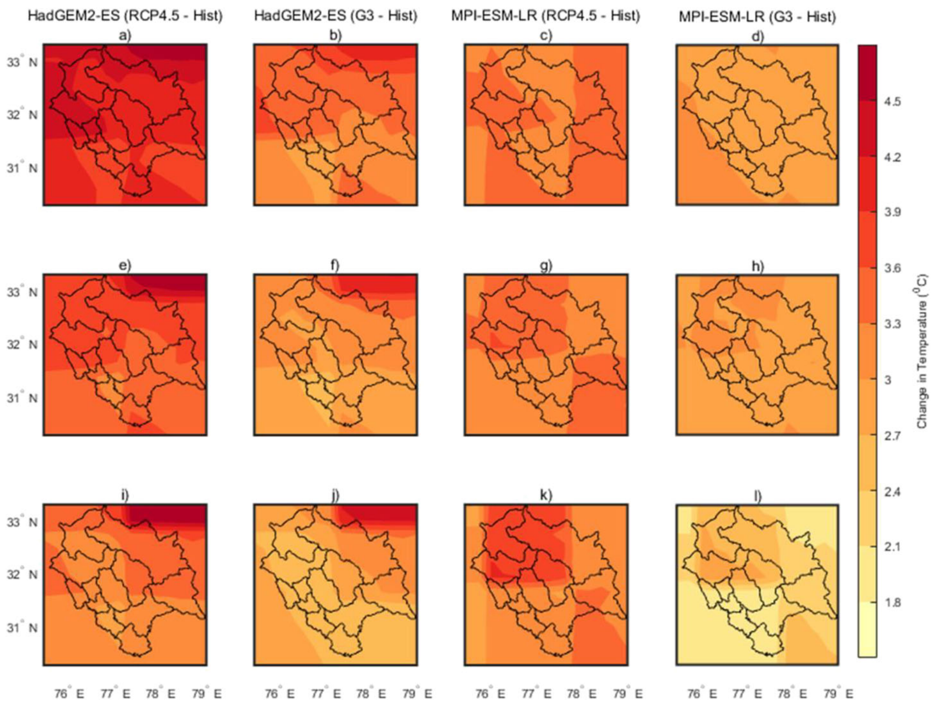

Fig. 4 Simulated changes in daily maximum temperature (a, b, c, d), daily mean temperature (e, f, g, h), and daily minimum temperature (i, j, k, l) under RCP4.5 and G3 for HadGEM2-ES and MPI-ESM-LR for period 2 (2075–2089; geoengineering switched off)

inadequately low GDH because of low temperatures. The deciduous fruits can be from various categories; some require high GDH and low CP (citrus fruits, grown in the region I), higher CP and moderate GDH (apple, chestnut), or a modest amount of CP and GDH (pear, peach, almonds). The spatial pattern of CP and GDH for HadGEM2-ES and MPI-ESM-LR is similar; however, winter chill differs somewhat in magnitude. HadGEM2-ES has low CP values in region III as compared with MPI-ESM-LR as a result of higher winter temperatures.

Figure 6 shows the spatial pattern of changes in CP (for the average of HadGEM2-ES and MPI-ESM-LR) under RCP4.5 and G3, for period 1 and period 2. The spatial patterns of

Table 1 Spatial range of differences in maximum, mean, and minimum temperatures between RCP4.5 and G3 simulations averaged for the end of the geoengineering period (1) and the end of the termination period (2) for Himachal Pradesh, India

	Daily maximum temperature (°C)		Daily mean temperature (°C)		Daily minimum temperature (°C)	
	RCP4.5-Hist	G3-Hist	RCP4.5-Hist	G3-Hist	RCP4.5-Hist	G3-Hist
Period 1 (2055–2069)						
HadGEM2-ES	2.7–3.5	1.8–2.4	2.4–3.4	1.7–2.3	2.5–3.5	1.5–3.1
MPI-ESM-LR	2.9–3.4	1.6–2.2	2.9–3.5	1.7–2.3	2.8–3.8	1.9–2.4
Period 2 (2075–2089)						
HadGEM2-ES	3.6–4.4	2.8–3.7	3.2–4.1	2.6–3.6	2.9–4.1	2.5–3.7
MPI-ESM-LR	3.1–3.5	2.7–3.1	3.0–3.6	2.8–3.2	2.8–3.9	1.9–3.8

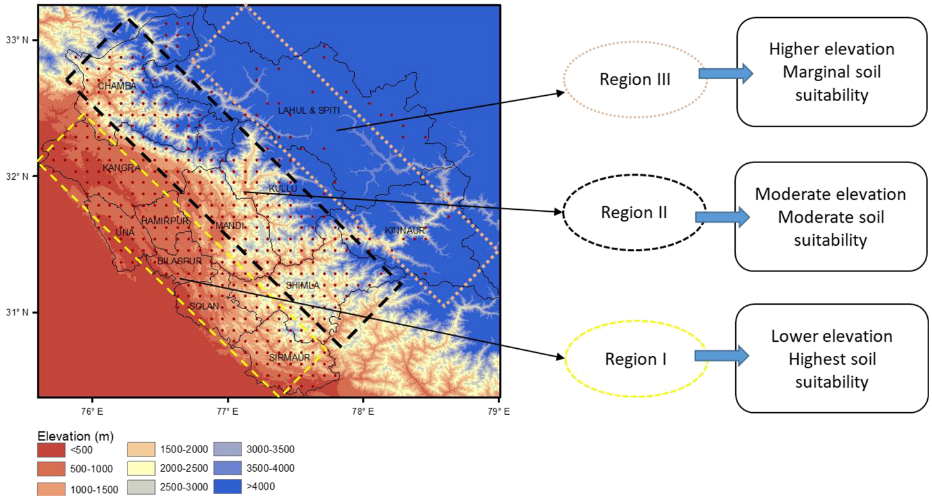

Fig. 5 Orography map of Himachal Pradesh derived from Shuttle Radar Topography Mission Digital Elevation Model at 1-km resolution showing elevation in meters, overlaid with suitable soil (red dots) and the three divided regions (I, II, and III)

changes in CP for HadGEM2-ES and MPI-ESM-LR (for period 1 and period 2) are plotted in Supplementary Fig. VI and VII, respectively. The summary from these three figures (Supplementary Fig. VI, VII, and Fig. 6) is tabulated in Table 2. MPI-ESM-LR shows a higher decline

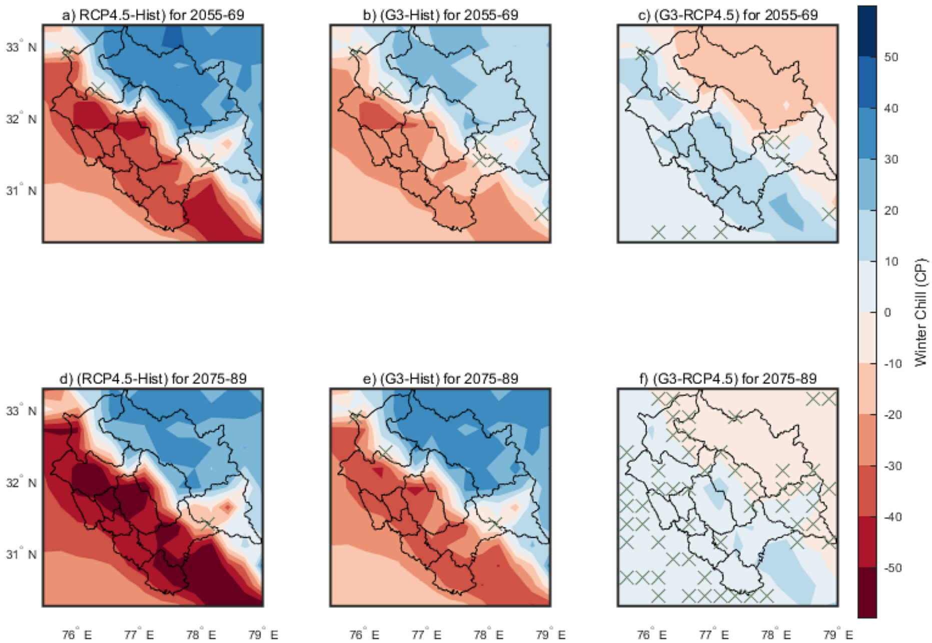

Fig. 6 Impact of global warming and geoengineering on chill accumulation (CP) in period 1 (a, b, c) and period 2 (d, e, f) for the average of HadGEM2-ES and MPI-ESM-LR over Himachal Pradesh, India. The unhatched area shows that the difference of CP for the given scenarios is statistically significant at 99% (for RCP4.5-Hist and G3-Hist) and 95% (G3-RCP4.5), according to the Wilcoxon rank-sum test

Table 2 Spatial range of differences in winter chill (CP) and growing degree hours (GDH) between historical, RCP4.5, and G3 simulations averaged for the end of the geoengineering period (1) and the end of the termination period (2) for Himachal Pradesh, India

	CP			GDH (× 10^3)		
	RCP4.5-Hist	G3-Hist	G3-RCP4.5	RCP4.5-Hist	G3-Hist	G3-RCP4.5
Period 1 (2055–2069)						
HadGEM2-ES	− 48–45	− 25–25	− 20–23	− 16.0–13.4	− 11.7–10.0	− 3.8–5.1
MPI-ESM-LR	− 53–43	− 42–30	− 14–21	− 21.6–17.9	− 11.1–11.0	− 7.8–9.5
Ensemble	− 49–43	− 33–27	− 17–22	− 18.6–15.3	− 11.2–10.2	− 5.7–7.3
Period 2 (2075–2089)						
HadGEM2-ES	− 59–48	− 44–45	− 13–17	− 20.0–16.0	− 17.5–14.1	− 2.1–3.5
MPI-ESM-LR	−55 – 43	− 46–36	− 10–13	− 20.8–18.2	− 19.4–16.0	− 2.6–2.6
Ensemble	− 53–45	− 43–39	− 10–15	− 20.0–16.7	− 18.2–15.0	− 2.1–2.4

in CP as compared with HadGEM2-ES for period 1; in period 2, CP values of MPI-ESM-LR increase slightly from period 1, whereas HadGEM2-ES CP values increase significantly in period 2. Under the RCP4.5 global warming scenario for period 1 (Fig. 6a), areas with high CP values are projected to shift northeastward as compared with Hist, especially reducing the climatically suitable areas of Shimla district and lower parts of Kullu district (region II). The winter chill in the region I is projected to decrease up to 40 CP, making large parts of it climatically unsuitable for the cultivation of deciduous fruits. In region III, the winter chill is projected to increase by approximately 40 CP in Lahaul and Spiti and decrease around 10–20 CP in Kinnaur district. There is a projected decrease of 10–30 CP in region II, with Shimla district witnessing the highest decline of 30 CP, followed by Kullu and Chamba districts (20 CP). Stratospheric geoengineering (G3) reduces the decline of winter chill in the region I and lower parts of region II up to 25 CP, suppresses the reduction by 15 CP in upper parts of region II, and slows the increase by almost 20 CP in Lahaul and Spiti (part of region III). Shimla district produces almost half the fruits (especially apple) in Himachal Pradesh, and such a decrease in winter chill accumulation would significantly impact the fruit production.

Figure 6 d, e, and f show the spatial pattern of changes in CP for period 2. Under RCP4.5 (Fig. 6d), the area with high CP values is projected to be shifted northeastward as compared with Hist, similar to Fig. 6a, but with a bit higher magnitude of change (around 45 CP). As geoengineering is switched off, the difference between G3 and RCP4.5 reduces to 10–15 CP (Fig. 6c). The winter chill is projected to decrease by up to 55 CP in lower parts of region II and around 5–25 CP in the Kinnaur district and increase by 45 CP in Lahaul and Spiti (Fig. 6a).

The spatial pattern of changes in GDH in RCP4.5 and G3 for period 1 and period 2 is plotted in Fig. 7. The same for HadGEM2-ES and MPI-ESM-LR is plotted in Supplementary Fig. VIII and IX, respectively. Figure 7 a–c represent the impact of global warming and geoengineering on heat accumulation for period 1. As can be seen from Fig. 7a, under RCP4.5, GDH is projected to decrease by up to 15,000 in lower-lying districts (region I), whereas, for regions II and III, it is projected to increase between 8000 and 18,000. Therefore, while the region I is projected to have an adverse impact, high-altitude areas (regions II and III) may benefit from global warming due to increased GDH. However, as can be seen in Fig. 7e,f, the application of geoengineering to RCP4.5 (G3) reduces the increase in GDH (in regions II, III by 5000–1000 GDH) and decreases in the region I (by 3000–7000 GDH). Figure 7 d–f show the spatial pattern of changes in CP and GDH for RCP4.5 and G3 for period 2. The spatial

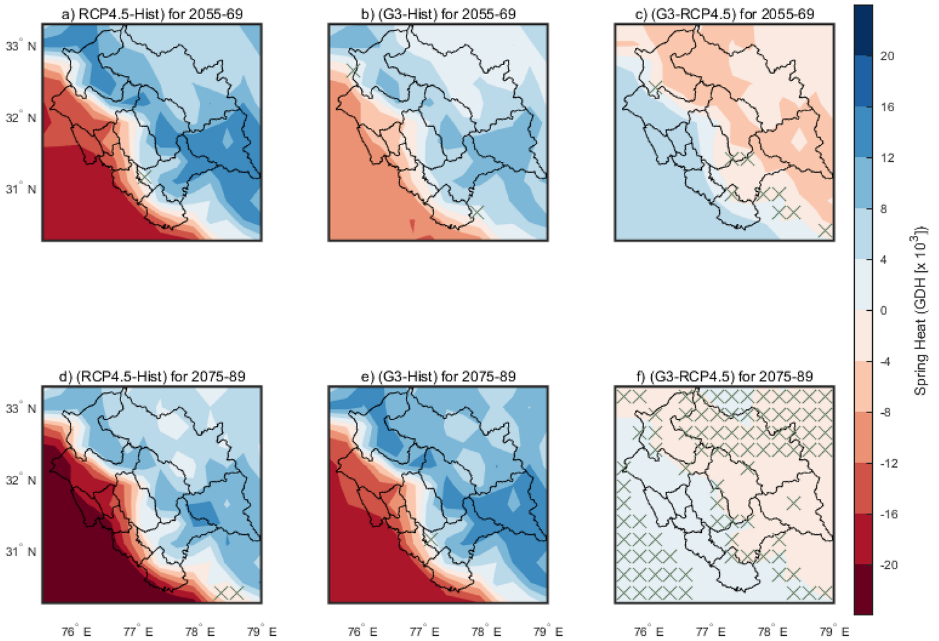

Fig. 7 Impact of global warming and geoengineering on heat accumulation (GDH) in period 1 (a, b, c) and period 2 (d, e, f) for the average of HadGEM2-ES and MPI-ESM-LR over Himachal Pradesh, India. The unhatched area shows that the difference of GDH for the given scenarios is statistically significant at 99% (for RCP4.5-Hist and G3-Hist) and 95% (G3-RCP4.5), according to the Wilcoxon rank-sum test

pattern of change in heat accumulation is almost similar to period 1, with intensification in magnitude. The difference between RCP4.5 and G3 is projected to reduce by up to 5000 GDH in the region I and 3000 GDH in region II and III after geoengineering is switched off (Fig. 7f).

3.3 Changes in agroclimatic and land suitability of deciduous fruit cultivation under RCP4.5 and G3

In this subsection, we investigate changes in the overall land suitability, comprising of agroclimatic suitability (taking both CP and GDH into account) and soil suitability, under RCP4.5 and G3. To delineate the agroclimatic suitability of the mentioned fruits, a threshold of CP and GDH was determined from the literature. The threshold indicates the minimum value above which the cultivation of mentioned deciduous fruits is possible. Adapted from the values specified by the University of California – Davis Fruit & Nut Research and Information web portal and Santos et al. (2017), CP greater than 50 is considered as the lower limit for chill requirement fulfillment. Similarly, GDH greater than 15,000 is taken as the lower limit of heat requirement (Ramirez-Villegas and Jarvis 2010; Guo et al. 2014). For a given grid, if 80% of the total years satisfy the threshold criteria of CP and GDH, it is considered agroclimatically suitable.

Figure 8 a–c represent agroclimatic suitability (for the average of HadGEM2-ES and MPI-ESM-LR) of deciduous fruits (citrus, apple, peach, cherry, walnut, and pistachio) in Hist, RCP4.5, and G3, respectively for period 1. The spatial pattern of changes in CP for HadGEM2-ES and MPI-ESM-LR is plotted in Supplementary Fig. X and XI, respectively, for the same period. The map of suitable soil is overlaid over the agroclimatic suitability map

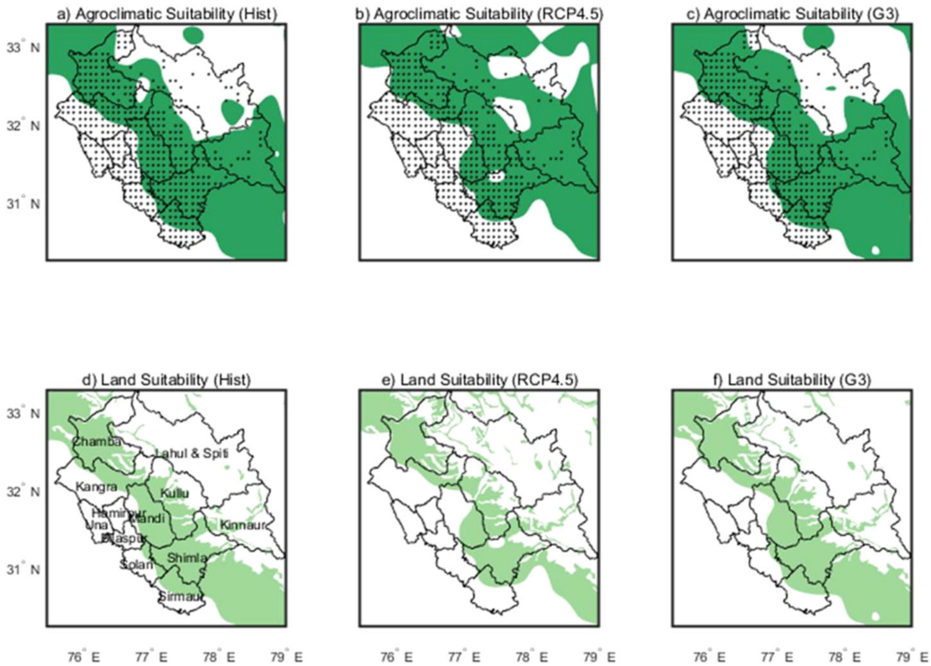

Fig. 8 Agroclimatic suitability (a, b, and c) and land suitability (d, e, and f) for period 1 (2055–2069) obtained from the average of HadGEM2-ES and MPI-ESM-LR. The regions having adequate climate to support agriculture is termed as agroclimatically suitable. The area having suitable soil (shown as black dots) is overlaid on a, b and c. Suitable climate is combined with suitable soil to delineate land suitability. The shaded area is the suitable region and the white area is the unsuitable region

to investigate if the areas undergoing beneficial agroclimatic change have suitable soil as well. In the figure, the green shaded region is a suitable area, and the transparent region depicts the unsuitable area. CP and GDH are combined by taking their intersection to map agroclimatic suitability. Region II (with high agroclimatic suitability for growing deciduous fruits in the present climate) is projected to become less suitable under RCP4.5, whereas region III (having low agroclimatic suitability for growing deciduous fruits in the present climate) is projected to become more suitable under RCP4.5. However, since region III has very less area with suitable soil, suitable climatic conditions because of global warming may not be beneficial. In other words under RCP4.5 and G3 (for period 1), the suitable area is projected to shift upwards, hence making the lower-lying areas (suitable in Hist) agroclimatically unsuitable. G3 seems to have a significant role in suppressing the change in RCP4.5 (compared with Hist). The total suitable area in Hist, RCP4.5, and G3 (Fig. 8a–c) remains almost similar because of the upper regions becoming suitable. Next, agroclimatic suitability is combined with suitable soils (texture, depth, and slope) to delineate the effective suitable land (see Fig. 8d–f). The effective suitable areas (arable) show a significant loss of arable land under RCP4.5. However, the role of G3 is significant in saving the arable lands, especially in Mandi and Shimla districts. The upper areas of region III have a tiny fraction of suitable soil and hence cannot compensate for the loss despite being agroclimatically suitable in RCP4.5. The loss of suitable lands is much higher in HadGEM2-ES compared with MPI-ESM-LR. However, in both models, G3 is able to save suitable lands considerably. Therefore, global warming (RCP4.5) is projected to have adverse impacts on the cultivation of deciduous fruits in Himachal Pradesh. However, geoengineering (G3) is expected to reduce the adverse impacts of global warming on deciduous fruit crop production, especially by altering the change in chill accumulation.

Figure 9 shows the spatial pattern of changes in agroclimatic and land suitability of deciduous fruits for RCP4.5 and G3 for period 2. It is projected that region I will become unsuitable; region II will witness a higher decline further, whereas almost entire region III will become agroclimatically suitable under RCP4.5 (Fig. 9b–c). Therefore, agroclimatically suitable areas are projected to shift more towards the northeast of the state. The total effective area is projected to reduce further in this period for RCP4.5 and G3 (Fig. 9e–f). The suitable agroclimatic area is bigger in RCP4.5 and G3 as compared with Hist. Nevertheless, the effective area is projected to reduce further, due to the unavailability of suitable soils in region III. After geoengineering is switched off, a higher fraction of arable land loss is projected due to global warming as the magnitude of benefits from G3 is projected to reduce sharply. However, G3 still is able to save the arable lands of Shimla and Mandi districts.

4 Summary and discussion

Given the utmost importance of near-surface air temperature during various phases in the life cycle of deciduous fruits, and the fact that global warming has a profound impact on temperature and its spatiotemporal distribution, the impact of RCP4.5 scenario on the projected daily maximum, mean, and minimum temperature over Himachal Pradesh is

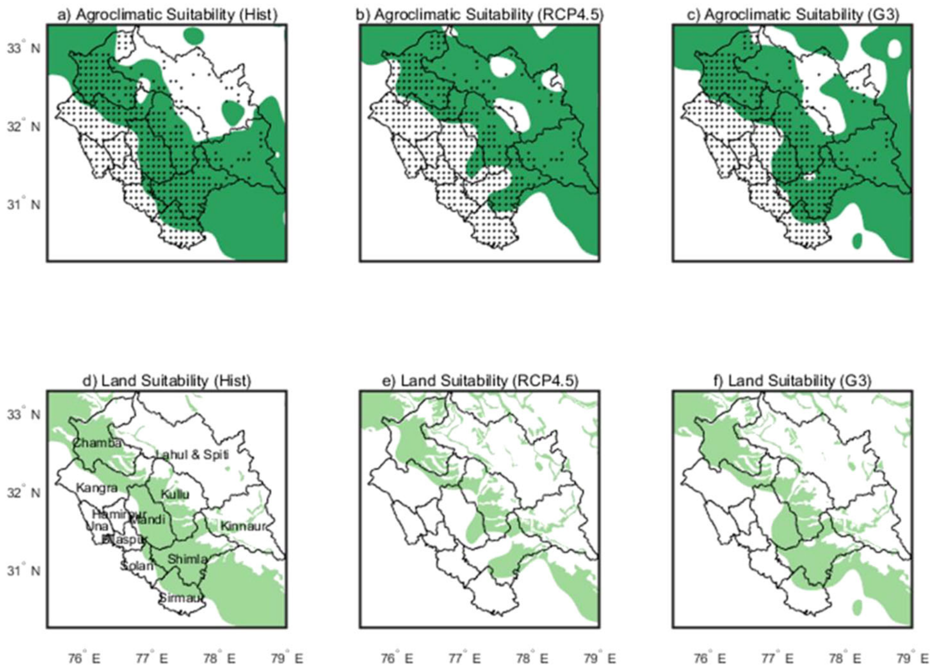

Fig. 9 Agroclimatic suitability (a, b, and c) and land suitability (d, e, and f) for period 2 (2075–2089) obtained from the average of HadGEM2-ES and MPI-ESM-LR. The regions having adequate climate to support agriculture is termed as agroclimatically suitable. The area having suitable soil (shown as black dots) is overlaid on a, b and c. Suitable climate is combined with suitable soil to delineate land suitability. The shaded area is the suitable region and the white area is unsuitable region

investigated, and the subsequent role of geoengineering in modulating the global warming impact is explored. The analysis is done for two 15-year periods, i.e., 2055–2069 (period 1; geoengineering switched on) and 2075–2089 (period 2; geoengineering switched off), considering that geoengineering was switched off in the model simulations starting 2070 and that the models were run till 2089. We used HadGEM2-ES and MPI-ESM-LR for this study.

The changes in temperature for both the models are not identical; MPI-ESM-LR exhibits higher warming as compared to HadGEM2-ES in period 1, whereas, in period 2, MPI-ESM-LR shows slight warming from period 1 (around 0.2 °C) and the rise is about 1 °C for HadGEM2-ES. However, the change in temperature under RCP4.5 and G3 is as high as 4.5 °C. Hence, the magnitude of the temperature difference between the models is much smaller. CP and GDH were used to assess the change in thermal growing conditions of deciduous fruit trees in Himachal Pradesh, under RCP4.5 and G3 for the two periods mentioned above. The study region is divided into three parts based on the topography, and changes are evaluated accordingly. Chill accumulation is projected to increase in RCP4.5 as compared with historical in higher (region III) elevations of the state, and decrease in mid (region II) and lower (region I) elevations, for both periods. Geoengineering seems to reduce the impact of warming on CP during the switched on period; however, the CP values under G3 seem to shift towards RCP4.5 once geoengineering is switched off. Heat accumulation is projected to increase over region III as well as II and decrease over the region I under RCP4.5 as well as G3 for both periods. However, for the later period, the intensity of change is higher, and the gap between G3 and RCP4.5 diminishes since geoengineering is switched off. The patterns of change in CP and GDH for RCP4.5 and G3 for period 1 and period 2 for both models follow similar characteristics as of daily temperature explained above. However, the magnitude of differences between HadGEM2-ES and MPI-ESM-LR amounts to only ~ 10% of the change due to global warming. Hence, the results discussed (average of HadGEM2-ES and MPI-ESM-LR) are robust.

The agroclimatically suitable area is projected to shift northeastwards (having higher elevations) under RCP4.5 as well as G3 for both periods. During the switched on period of 2055–2069, geoengineering restricts the shift; hence, the currently suitable areas of Shimla and Mandi districts are not lost in G3. During the switched off period of 2075–2089, the projected shift is intensified under RCP4.5. Even after geoengineering is switched off, G3 is able to save areas of region II (Shimla and Mandi districts) that are the major producers of deciduous fruits in the current climate. During the switched on period of 2055–2069, the total agroclimatically suitable area remains almost the same under RCP4.5 as well as G3, although there is a northeastward shift; however, the effective suitable area (taking into account the soil suitability along with agroclimatic suitability) is projected to significantly reduce under RCP4.5, but G3 seems to partially nullify this effect. During the switched off period of 2075–2089, the total agroclimatically suitable area again remains almost the same under RCP4.5 as well as G3, although with a northeastward shift; however, the effective suitable area is projected to shrink even further under RCP4.5, and the effect of G3 is much less as compared with the switched on period. In both period 1 and period 2, the agroclimatically suitable area would shrink in the region I and region II and expands in region III. For an area to become cultivable, it should have a favorable climate along with good soil. However, suitable soils cover only a tiny fraction (around 10–15%) of region III. Hence, a future favorable climate in region III cannot compensate for the lost suitable lands of the regions I and II. However, overall, geoengineering is found to play a positive role in saving lower elevations of the state from becoming unsuitable due to global warming. In fact, even after geoengineering is switched off, areas of Shimla would remain suitable under G3.

Thus, we find that the areas that are suitable in the current climate are projected to become less suitable or unsuitable under global warming, leading to reduced yields. Although geoengineering is found to reduce the impact of global warming on the effective suitable area for deciduous fruit cultivation, it does not completely nullify the effect. The high-chill demanding temperate fruits may no longer be suitable for the given location and may have to be replaced by low-chill requiring fruits or vegetables. In lower-lying areas of Kullu district, most of the high-chill demanding fruits species are already getting replaced by low-chill requiring fruits and vegetables because of degradation in the quality of high-chill demanding temperate fruits such as apple as a result of global warming (Vedwan and Rhoades 2001). Pre-established orchards may witness a decline in productivity in the future. It would thus be necessary to introduce new fruit and vegetable species suitable for the changing climate to avoid a total failure. The life span of an orchard is around 40 years, and it takes 3–5 years to start producing fruits in new orchards. Unlike seasonal crops such as rice, wheat, and maize, orchards are costly and therefore suffer much higher losses in both time and cost as a result of climate change. In the RCP4.5 scenario, the productivity of deciduous fruit orchards decreases because of low winter chill, and at some point of time, the orchards may stop producing. Geoengineering would help to reduce the magnitude of these adverse conditions, but it would not compensate for many of the impacts of global warming. If geoengineering were terminated, the climate would rapidly warm to match the RCP4.5 scenario. This could cause a much more substantial shift in the land suitability regime in a short period and possibly be more adverse than global warming under the RCP4.5 scenario.

G3 is only one possible geoengineering scenario that might be implemented. The results presented here would have to be scaled for stronger or weaker scenarios. In a scenario like G3, in which radiative forcing is kept from changing to minimize the increase in global mean temperatures in spite of increases in greenhouse gases, the orchards established currently would not witness significant changes in productivity while geoengineering was on. However, if geoengineering were terminated, the rate of change in warming would be quite high, and it could lead to total crop failure in a shorter period. However, if moderate geoengineering were implemented that reduces the global warming, say, by 1 °C, it may not reduce the changes much but could make the shift from current orchards to suitable future options much more gradual for the farmers, and once the geoengineering is stopped, the rate of change in temperature would not be that high. Gradual termination of geoengineering could reduce the abrupt high rate of changes in temperature and would be less harmful to the fruit orchards, but this cannot be guaranteed, and it is easy to think of scenarios that would result in abrupt termination.

To the best of our knowledge, this is the first study to investigate the impact of geoengineering on the cultivation of deciduous fruits. However, there have been studies on the effects of global warming on deciduous fruit production (Luedeling et al. 2009b, a; Luedeling 2012; Rana et al. 2015; Santos et al. 2017). The change in the suitability of deciduous fruit cultivation under global warming aligns with the above research. We used climate model daily temperatures, converted them from daily to hourly temporal resolution, and used the hourly temperatures to compute chill and heat accumulation to assess changes in thermal growing requirements of the deciduous fruits. Soil suitability to practice cultivation was also taken into consideration to get the effective area available for establishing deciduous fruit orchards. Himachal Pradesh has a hilly terrain, and the pattern of spatial changes in chill and heat accumulation reported in the current study may not directly apply to other regions. However, the results regarding the shrinking of presently suitable lands for deciduous fruits under global warming are general, as depicted by other studies as well.

There are uncertainties in our study. We have used a statistical downscaling technique because of the unavailability of high-resolution climate models apt for this study. A critical limitation of downscaling is the inability to capture extreme events such as heatwaves, cold snaps, floods, and droughts. So, the results of this study may not represent the accurate picture if extreme temperature events become the new normal. The daily temperature was converted to hourly using a model because of the absence of hourly temperature simulations from climate models. We fed the hourly temperature data into models to compute CP and GDH. We have tried to use the best suitable models for the region to compute these parameters. To quantify the errors, we would need the observed hourly temperature data from various locations of Himachal Pradesh. However, because of the lack of observed data, we were not able to do this. The use of various methods in this study may lead to some error propagation, but we used the best possible methodology we could follow because of data limitations in the current scenario. However, we have no evidence that the potential errors in each step of our work are correlated, so are not concerned with error growth. The results presented here are based on simulations from two models (HadGEM2-ES and MPI-ESM-LR), and they both gave similar results, suggesting that the results are not model dependent. The analysis has been carried out for one global warming scenario (RCP4.5) and one stratospheric geoengineering scenario (G3), as described in the data and methodology section, but as discussed above, they could be scaled for other scenarios. Because we only addressed one crop type in one region of the world, more studies would be required to have a more holistic picture, in order to help the global community make a more informed decision on whether to implement such large-scale climate engineering.

Acknowledgments Prof. S. K. Mishra is thankfully acknowledged for discussions. Alan Robock is supported by the US National Science Foundation grant AGS-1617844. We acknowledge NBSS, the Princeton hydrology group, CMIP, and GeoMIP, for making the data available.

References

Atkinson CJ, Brennan RM, Jones HG (2013) Declining chilling and its impact on temperate perennial crops. Environ Exp Bot 91:48–62. https://doi.org/10.1016/j.envexpbot.2013.02.004

Becker JJ, Sandwell DT, Smith WHF et al (2009) Global bathymetry and elevation data at 30 arc seconds resolution: SRTM30_PLUS. Mar Geod 32:355–371. https://doi.org/10.1080/01490410903297766

Bhagat RM, Singh S, Sood C et al (2009) Land suitability analysis for cereal production in Himachal Pradesh (India) using Geographical Information System. J Indian Soc Remote Sens 37:233–240. https://doi.org/10.1007/s12524-009-0018-6

Cesaraccio C, Spano D, Duce P, Snyder RL (2001) An improved model for determining degree-day values from daily temperature data. Int J Biometeorol 45:161–169

Cesaraccio C, Spano D, Snyder RL, Duce P (2004) Chilling and forcing model to predict bud-burst of crop and forest species. Agric For Meteorol 126:1–13. https://doi.org/10.1016/j.agrformet.2004.03.002

Chandler WH (1942) Deciduous orchards. H. Kimpton, London (printed in America)

Chaudhary P, Bawa KS (2011) Local perceptions of climate change validated by scientific evidence in the Himalayas. Biol Lett 7:767–770. https://doi.org/10.1098/rsbl.2011.0269

Collins WJ, Bellouin N, Doutriaux-Boucher M et al (2011) Development and evaluation of an Earth-System model – HadGEM2. Geosci Model Dev 4:1051–1075. https://doi.org/10.5194/gmd-4-1051-2011

Dash SK, Hunt JCR (2007) Variability of climate change in India. Curr Sci 93:782–788

Erez A (2000) Bud dormancy; phenomenon, problems and solutions in the tropics and subtropics. In: Temperate fruit crops in warm climates. Springer Netherlands, Dordrecht, pp 17–48

Erez A, Fishman S, Linsley-Noakes GC, Allan P (1990) The dynamic model for rest completion in peach buds. Acta Hortic:165–174. https://doi.org/10.17660/ActaHortic.1990.276.18

Ferraro AJ, Griffiths HG (2016) Quantifying the temperature-independent effect of stratospheric aerosol geoengineering on global-mean precipitation in a multi-model ensemble. Environ Res Lett 11:034012. https://doi.org/10.1088/1748-9326/11/3/034012

Fishman S, Erez A, Couvillon GA (1987) The temperature dependence of dormancy breaking in plants: mathematical analysis of a two-step model involving a cooperative transition. J Theor Biol 124:473–483. https://doi.org/10.1016/S0022-5193(87)80221-7

Ghosh SP (1999) Deciduous fruit production in India. Deciduous fruit production in Asia and the Pacific, In, pp 38–56

Giorgetta MA, Jungclaus J, Reick CH et al (2013) Climate and carbon cycle changes from 1850 to 2100 in MPI-ESM simulations for the Coupled Model Intercomparison Project phase 5. J Adv Model Earth Syst 5:572–597. https://doi.org/10.1002/jame.20038

Gudmundsson L, Bremnes JB, Haugen JE, Engen-Skaugen T (2012) Downscaling RCM precipitation to the station scale using statistical transformations–a comparison of methods. Hydrol Earth Syst Sci 16:3383–3390. https://doi.org/10.5194/hess-16-3383-2012

Guo L, Dai J, Ranjitkar S et al (2014) Chilling and heat requirements for flowering in temperate fruit trees. Int J Biometeorol 58:1195–1206. https://doi.org/10.1007/s00484-013-0714-3

Guo L, Xu J, Dai J et al (2015) Statistical identification of chilling and heat requirements for apricot flower buds in Beijing, China. Sci Hortic (Amsterdam) 195:138–144. https://doi.org/10.1016/j.scienta.2015.09.006

Ikinci A, Mamay M, Unlu L et al (2014) Determination of heat requirements and effective heat summations of some pomegranate cultivars grown in Southern Anatolia. Erwerbs-Obstbau 56:131–138. https://doi.org/10.1007/s10341-014-0220-8

IPCC (2014) Climate Change 2014: Mitigation of Climate Change. In: Edenhofer O, Pichs-Madruga R, Sokona Y, Farahani E, Kadner S, Seyboth K, Adler A, Baum I, Brunner S, Eickemeier P, Kriemann B, Savolainen J, Schlömer S, von Stechow C, Zwickel T, Minx JC (eds) Contribution of Working Group III to the Fifth Assessment Report of the Intergovernmental Panel on Climate Change. Cambridge University Press, Cambridge and New York

Kihoro J, Bosco NJ, Murage H (2013) Suitability analysis for rice growing sites using a multicriteria evaluation and GIS approach in great Mwea region, Kenya. Springerplus 2:1–9. https://doi.org/10.1186/2193-1801-2-265

Kishore DK, Pramanick KK, Singh AK et al (2015) Chilling unit accumulation at Shimla, Himachal Pradesh, India—a predominantly apple (Malus × domestica Borkh) growing region. Int J Fruit Sci 15:117–128. https://doi.org/10.1080/15538362.2014.931171

Kravitz B, Robock A, Boucher O et al (2011) The geoengineering model intercomparison project (GeoMIP). Atmos Sci Lett 12:162–167. https://doi.org/10.1002/asl.316

Linkosalo T (2000) Mutual regularity of spring phenology of some boreal tree species: predicting with other species and phenological models. Can J For Res 30:667–673. https://doi.org/10.1139/x99-243

Linvill D (1990) Calculating chilling hours and chill units from daily maximum and minimum temperature observations. HortScience 25:14–16

Luedeling E (2012) Climate change impacts on winter chill for temperate fruit and nut production: a review. Sci Hortic (Amsterdam) 144:218–229. https://doi.org/10.1016/j.scienta.2012.07.011

Luedeling E, Brown PH (2011) A global analysis of the comparability of winter chill models for fruit and nut trees. Int J Biometeorol 55:411–421. https://doi.org/10.1007/s00484-010-0352-y

Luedeling E, Zhang M, Girvetz EH (2009a) Climatic changes lead to declining winter chill for fruit and nut trees in California during 1950–2099. PLoS One 4:e6166. https://doi.org/10.1371/journal.pone.0006166

Luedeling E, Zhang M, Luedeling V, Girvetz EH (2009b) Sensitivity of winter chill models for fruit and nut trees to climate change. Agric Ecosyst Environ 133:23–31

Mann ME, Bradley RS, Hughes MK (1998) Global-scale temperature patterns and climate forcing over the past six centuries. Nature 392:779–787. https://doi.org/10.1038/33859

Mishra SK, Sahany S, Salunke P et al (2018) Fidelity of CMIP5 multi-model mean in assessing Indian monsoon simulations. npj Clim Atmos Sci 1:39. https://doi.org/10.1038/s41612-018-0049-1

Olesen JE, Bindi M (2002) Consequences of climate change for European agricultural productivity, land use and policy. Eur J Agron 16:239–262

Pérez FJ, Ormeño NJ, Reynaert B, Rubio S (2008) Use of the dynamic model for the assessment of winter chilling in a temperate and a subtropical climatic zone of Chile. Chil J Agric Res 68:198–206. https://doi.org/10.4067/s0718-58392008000200010

Pongratz J, Lobell DB, Cao L, Caldeira K (2012) Crop yields in a geoengineered climate. Nat Clim Chang 2:101–105. https://doi.org/10.1038/nclimate1373

Ramirez-Villegas J, Jarvis A (2010) Downscaling Global Circulation Model Outputs: The Delta Method Decision and Policy Analysis Working Paper No. 1

Rana RS, Bhagat RM, Kalia V, Lal H (2015) The impact of climate change on a shift of the apple belt in Himachal Pradesh. In: Handbook of Climate Change and India. Routledge
Renton A (2009) Suffering the science: climate change, people, and poverty. Oxfam Policy Pract Clim Chang Resil 5:53–113
Richardson E, Seeley S, Walker D (1974) A model for estimating the completion of rest for "Redhaven" and "Elberta" peach trees. HortScience 9:331–332
Robock A (2016) Albedo enhancement by stratospheric sulfur injections: more research needed. Earth's Futur 4: 644–648. https://doi.org/10.1002/2016EF000407
Santos JA, Costa R, Fraga H (2017) Climate change impacts on thermal growing conditions of main fruit species in Portugal. Clim Chang 140:273–286. https://doi.org/10.1007/s10584-016-1835-6
Schwartz MD, Hanes JM (2010) Continental-scale phenology: warming and chilling. Int J Climatol 30:1595–1598. https://doi.org/10.1002/joc.2014
Sehgal JL (1990) Soil resource mapping of different states of India: why and how?
Sheffield J, Goteti G, Wood EF (2006) Development of a 50-year high-resolution global dataset of meteorological forcings for land surface modeling. J Clim 19:3088–3111. https://doi.org/10.1175/JCLI3790.1
Shrestha UB, Gautam S, Bawa KS (2012) Widespread climate change in the Himalayas and associated changes in local ecosystems. PLoS One:7. https://doi.org/10.1371/journal.pone.0036741
Singh J, Patel NR (2017) Assessment of agroclimatic suitability of apple orchards in Himachal Pradesh under changing climate. J Agrometeorol 19:110–113
Srivastava AK, Rajeevan M, Kshirsagar SR (2009) Development of a high resolution daily gridded temperature data set (1969-2005) for the Indian region. Atmos Sci Lett 10:249–254. https://doi.org/10.1002/asl.232
Taylor KE, Stouffer RJ, Meehl GA (2012) An overview of CMIP5 and the experiment design. Bull Am Meteorol Soc 93:485–498
Tuan NT, Qiu J, Verdoodt A et al (2011) Temperature and precipitation suitability evaluation for the winter wheat and summer maize cropping system in the Huang-Huai-Hai Plain of China. Agric Sci China 10:275–288. https://doi.org/10.1016/S1671-2927(11)60005-9
Vedwan N, Rhoades RE (2001) Climate change in the western Himalayas of India: a study of local perception and response. Clim Res 19:109–117. https://doi.org/10.3354/cr019109
Xia L, Robock A, Cole J et al (2014) Solar radiation management impacts on agriculture in China: a case study in the Geoengineering Model Intercomparison Project (GeoMIP). J Geophys Res Atmos 119:8695–8711. https://doi.org/10.1002/2013JD020630
Yang H, Dobbie S, Ramirez-Villegas J et al (2016) Potential negative consequences of geoengineering on crop production: a study of Indian groundnut. Geophys Res Lett 43:11,786–11,795. https://doi.org/10.1002/2016GL071209
Yasutomi N, Hamada A, Yatagai A (2011) Development of a long-term daily gridded temperature dataset and its application to rain / snow discrimination of daily precipitation. Glob Environ Res 15:165–172

Affiliations

Jyoti Singh[1] • Sandeep Sahany[1,2] • Alan Robock[3]

✉ Jyoti Singh
ijyotikashyap@gmail.com

✉ Sandeep Sahany
ssahany@cas.iitd.ac.in

1 Present address: Centre for Atmospheric Sciences, Indian Institute of Technology Delhi, 337, Block-VI, Hauz Khas, New Delhi 110016, India

2 Centre for Climate Research, Singapore, Singapore

3 Department of Environmental Sciences, Rutgers University, New Brunswick, NJ, USA